Malaysian Journal of Chemistry, 2026, Vol. 28(2), 67-79

Unveiling the Antioxidant Potential of Aspidxanthone A: A Theoretical Insight

Hoang Thi Tue Trang[1], Ngu Thi Tra Giang[2] and Nguyen Ngoc Anh Thu[3]*
[1]Department of Chemistry, Hanoi Architectural University, Hanoi, Vietnam
[2]Department of Chemistry, Vinh University, Vinh City, Nghean, Vietnam
[3]Department of Chemical Engineering, School of Chemistry and Life Sciences, Hanoi University of Science and Technology, 1 Dai Co Viet, Hai Ba Trung, Hanoi, Vietnam
Correspondence author (e-mail: thu.nna281@gmail.com)

Aspidistra letreae, a species found only in central Vietnam, contains diverse bioactive compounds. Among them, aspidxanthone A (AL) has shown notable antioxidant activity. In this study, we used a multi-scale computational strategy to explore how AL exerts its antioxidant effects at the molecular level. Thermodynamic and kinetic analyses revealed that AL scavenged hydroperoxyl radicals primarily through the single electron transfer (SET) mechanism in aqueous environments. The O17 hydroxyl group stood out as the most reactive site, supported by its favourable ionization potential and a total rate constant of 1.28×10^7 $M^{-1}.s^{-1}$. In contrast, in lipid-like environments such as pentylethanoate, the hydrogen atom transfer (HAT) mechanism predominated. Molecular docking simulations demonstrated that AL bound strongly to the Keap1 protein (–9.108 kcal/mol), forming stable interactions with key residues like Tyr334 and Ser363. Compared to known natural antioxidants, AL showed superior binding affinity. Molecular dynamics simulations confirmed the stability of the Keap1–AL complex, suggesting that AL may disrupt the Keap1–Nrf2 interaction and thereby strengthen antioxidant defences. ADMET predictions indicated good oral absorption and safety, though mutagenicity and poor CNS penetration remained limitations. To the best of our knowledge, this work represents the first comprehensive computational characterization of AL as a dual-mode antioxidant, combining radical-scavenging reactivity with Keap1 inhibition. Overall, AL emerges as a promising antioxidant lead compound with dual radical-scavenging and Keap1-inhibitory activity, supporting its further development for treating oxidative stress-related diseases.

Keywords: Aspidxanthone A, *Aspidistra letreae*, thermodynamic, kinetic, molecular docking, molecular dynamics.

Received: September 2025; Accepted: January 2026

Aspidistra letreae Aver., Tillich & T.A. Le, first discovered in 2016, is an endemic plant species native to the central region of Vietnam [1]. This species has garnered significant scientific interest due to its phytochemical profile, which includes xanthones, steroid saponins, spirostanol saponins, glyceryl glucosides, coumarins, tocopherols, and other secondary metabolites [2, 3, 4]. These compounds have shown a wide range of biological activities, notably antioxidant, cytotoxic, and anticancer effects [2, 4, 5]. Among them, aspidxanthone A (AL) has emerged as a promising molecule (Figure 1) [4]. Recently isolated from *A. letreae* for the first time, AL exhibited remarkable antioxidant capacity, with a DPPH radical scavenging IC_{50} value of 11.2 μM comparable to the standard antioxidant ascorbic acid (IC_{50} = 9.83 μM) [4]. This initial discovery underscores the potential of AL as a lead compound in the development of novel antioxidant agents. Despite its potent *in vitro* antioxidant performance, the molecular mechanisms underlying AL's antioxidant activity have yet to be fully explored. Unlike many other xanthones, AL features a unique substitution pattern characterized by a rare combination of prenyl and hydroxyl groups. These structural elements may enhance radical stabilization and reactivity, but their precise mechanistic contributions remain unclear. To date, no study has systematically examined how these structural features influence its thermodynamic feasibility and kinetic efficiency toward various reactive oxygen species (ROS). Moreover, while several xanthones have been computationally analyzed, AL has not yet undergone a dedicated mechanistic investigation that connects its molecular structure to its experimentally observed antioxidant potency. Addressing this gap is crucial to determine whether AL's superior DPPH scavenging activity originates from intrinsic electronic effects, favourable reaction energetics, or specific enzyme-target interactions. To bridge this knowledge gap, the present study aimed to systematically investigate the reaction mechanisms and kinetics of AL with key ROS, particularly the hydroperoxyl radical (HOO•), under physiologically relevant conditions [6, 7, 8]. A multi-scale computational approach was employed because no single method can fully capture the

complexity of antioxidant processes. Quantum chemical calculations were used to probe the thermodynamics and kinetics of radical scavenging at the atomic level, identifying the most favourable pathways. Computational kinetic modelling quantified rate constants under physiological conditions, linking molecular reactivity to potential biological relevance. Complementarily, molecular docking and molecular dynamics (MD) simulations evaluated the non-covalent interactions and inhibitory potential of AL toward the Keap1 protein, a central regulator in the Nrf2-mediated antioxidant defense pathway [9]. Through this multi-faceted computational approach, we sought to provide a molecular-level insight into the antioxidant behaviour of AL and its interaction with key biological targets in order to enhance our fundamental understanding of AL's bioactivity and pave the way for future *in vitro* and *in vivo* investigations, with the long-term goal of developing effective antioxidant or chemopreventive therapeutics derived from *Aspidistra letreae*.

COMPUTATIONAL DETAILS

In the present study, the geometries of the neutral molecule aspidxanthone A (Figure 1), its free radicals, cationic radicals, and anions were optimized using density functional theory (DFT) with the Minnesota density functional, M05-2X. The 6-311++G(d,p) basis set was employed in all calculations, and open-shell species were treated using the unrestricted formalism. Vibrational frequency calculations at the same level of theory were carried out to confirm that the optimized structures corresponded to energy minima, to evaluate zero-point energy corrections, and to determine thermal quantities. Solvent effects in this study, including water (ε = 78.35) as a representative of polar media and phenylethanoate as a lipid medium, were applied using the solvation model based on density (SMD) [10]. The free energy and enthalpy of the hydrogen atom and electron used in the calculations were obtained from a reference [11].

In the thermochemical study, three widely accepted mechanisms were considered for investigating antioxidant reactions: formal hydrogen atom transfer (fHAT), single electron transfer-proton transfer (SET-PT), and sequential proton loss electron transfer (SPLET).

1. The fHAT mechanism involves the O–H bond dissociation of AL–OH, and the characteristic quantity commonly used to describe this mechanism is the bond dissociation enthalpy (BDE):

$$BDE = H(AL\text{-}O^{\cdot}) + H(H^{\cdot}) - H(AL\text{-}OH)$$

2. The key thermodynamic parameter that characterizes the SET-PT mechanism is the ionization potential (IP).

$$IP = H(AL\text{-}OH^{\cdot+}) + H(e^{-}) - H(AL\text{-}OH)$$

3. The main parameter used to evaluate the sequential proton loss electron transfer (SPLET) mechanism is the proton affinity (PA).

$$PA = H(AL\text{-}O^{-}) + H(H^{+}) - H(AL\text{-}OH)$$

For the kinetic process, the reaction rate constant (k) was calculated based on conventional transition state theory (TST). The rate constant k for radical scavenging reactions has previously been reported [6]. All calculations were performed using the Gaussian 09 software package [12].

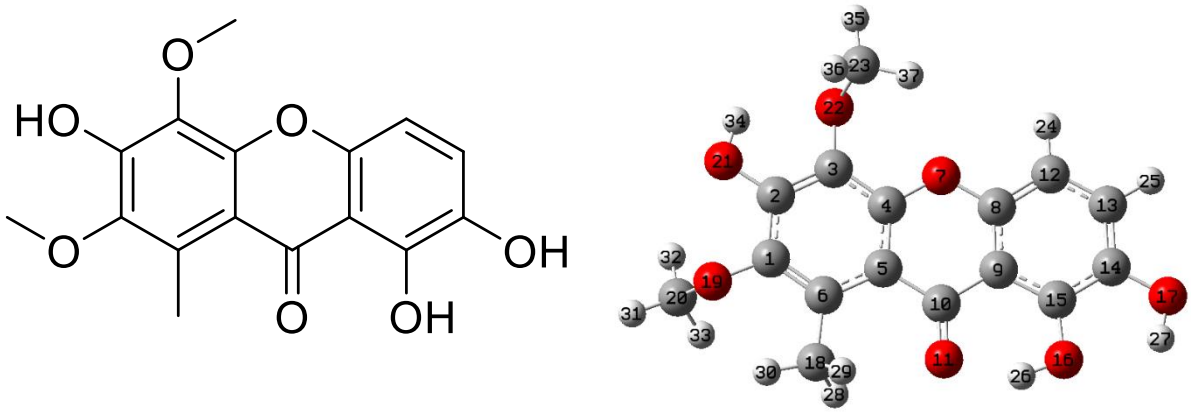

Figure 1. The molecular structure of compound AL, along with its atom numbering scheme.

Molecular Docking

The three-dimensional structure of the Keap1 protein in complex with (1S,2R)-2-{[(1S)-1-[(1,3-dioxo-1,3-dihydro-2H-isoindol-2-yl)methyl]-3,4-dihydro-isoquinolin-2(1H)-yl]carbonyl}cyclohexanecarboxylic acid (1VV) was retrieved from the Protein Data Bank (PDB ID: 4L7B) at a resolution of 2.41 Å [13]. Subsequently, water molecules were removed, the co-crystallized ligand was separated, polar hydrogens were added, and the structure was saved in PDBQT format using PyMOL and AutoDockTools software. For ligand preparation, the optimized structures of aspidxanthone A (AL) and the reference compound 1VV were prepared for docking simulations using the AutoDockTools software. Molecular docking was performed using the AutoDock Vina v1.2.3 program, with the docking parameters set following previous reports [6, 14]. Specifically, the grid box was positioned at the centre of the binding pocket corresponding to the co-crystallized ligand, using coordinates x = −2.636 Å, y = 3.267 Å, and z = −27.443 Å. It was defined with dimensions of 24 Å × 24 Å × 24 Å and a grid spacing of 1 Å. The protein-ligand interaction profiles after docking were visualized using the BIOVIA Discovery Studio Visualizer software.

Molecular Dynamics

The ligand-protein complexes were subjected to molecular dynamics (MD) simulations to evaluate the stability and dynamic behaviour of the ligand-bound protein systems [15, 16]. These simulations were performed using the GROMACS 2023.3 software package by applying an AMBER99SB-ILDN force field for the Keap1 protein (PDB ID: 4L7B) [17, 18]. For the ligands, parameters were generated using the General AMBER Force Field 2 (GAFF2) through the AmberTools23 suite to ensure compatibility with AMBER-based force fields [19, 20]. Each complex was solvated in a TIP3P water model box, and the systems were neutralized by adding suitable amounts of Na^+ and Cl^- ions. To eliminate unfavourable steric clashes between the protein, water molecules, and ions, an initial energy minimization of 50,000 steps using the steepest descent algorithm was carried out. During this process, protein atoms were restrained with a harmonic force constant of 1000 $kcal \cdot mol^{-1} \cdot Å^{-2}$ to allow the solvent to equilibrate around the protein. The systems were then equilibrated in two consecutive phases: 100 ps under the NVT ensemble (constant particle number, volume, and temperature) followed by 100 ps under the NPT ensemble (constant particle number, pressure, and temperature), both at 300 K and 1 atm. Temperature and pressure control were maintained using the Berendsen thermostat and the Parrinello-Rahman barostat, respectively. Hydrogen bond constraints were applied using the LINCS algorithm, enabling a 2 fs integration timestep during the MD simulations [21]. Short-range nonbonded interactions, including van der Waals and Coulomb forces, were evaluated with a 1.2 nm cutoff, while long-range electrostatic interactions were computed using the Particle-Mesh Ewald (PME) method. After equilibration, 100 ns of production MD simulations were conducted without positional restraints on the protein atoms. Throughout the simulations, a key structural parameter, root-mean-square deviation (RMSD) was monitored and visualized using XMGRACE software to provide detailed insights into the dynamic stability of the ligand-protein complexes.

ADMET Prediction

In silico ADMET prediction has become an indispensable component of modern drug discovery, offering rapid and cost-effective evaluation of pharmacokinetic and toxicity profiles. These computational methods allow researchers to assess the drug-likeness of chemical compounds early in the design process, thereby reducing reliance on time-consuming and expensive experimental testing. Among the widely used tools, pkCSM (http://biosig.unimelb.edu.au/pkcsm/prediction) stands out for its ability to predict a broad range of ADMET properties using graph-based signatures and machine learning algorithms. By analyzing a compound's molecular structure, pkCSM can provide valuable insights into absorption, distribution, metabolism, excretion, and toxicity, which are critical for identifying and optimizing lead compounds [22]. This approach streamlines the development pipeline and enhances the likelihood of success in later stages of drug development.

RESULTS AND DISCUSSION

Thermodynamic Results

Thermodynamic parameters played a pivotal role in elucidating the antioxidant mechanisms of AL, offering critical insights into its reactivity under diverse environmental conditions. Among these descriptors, bond dissociation enthalpy (BDE), ionization potential (IP), and proton affinity (PA) served as key benchmarks for evaluating the formal hydrogen atom transfer (fHAT), single electron transfer (SET), and sequential proton loss electron transfer (SPLET) mechanisms, respectively [23, 24].

For the fHAT mechanism, BDE was the principal determinant, with lower BDE values reflecting a greater capacity for hydrogen atom donation. In the gas phase, AL exhibited BDE values of 91.98, 86.75, and 88.17 kcal/mol at the O16, O17, and O21 positions, respectively, with O17–H displaying the lowest BDE, underscoring its superior hydrogen-donating ability (Table 1). In aqueous solution, BDE values further decreased to 86.12, 83.21, and 89.85 kcal/mol at O16, O17, and O21, respectively, highlighting the role of polar solvents in stabilizing the transition state and facilitating fHAT. In pentylethanoate, a moderate polar environment, BDE values were 88.96, 83.75, and 87.58 kcal/mol, again positioning O17 as the most reactive site.

With the SET mechanism, IP emerged as a critical parameter [25]. In the gas phase, AL showed consistently high IP values (~171.63 kcal/mol), which dramatically decreased in water (115.30 kcal/mol) and pentylethanoate (127.42 kcal/mol), reflecting the enhanced feasibility of electron donation in polar environments (Table 1). Notably, the O17 site maintained one of the lowest IP values across all media, reinforcing its central role in SET-mediated antioxidant activity.

For the SPLET mechanism, PA served as an essential descriptor [26]. In the gas phase, PA values ranged from 322.15 to 345.37 kcal/mol, with O17 again demonstrating the lowest PA, indicative of its enhanced proton-donating capacity (Table 1). In aqueous media, PA values sharply declined to 27.70–35.74 kcal/mol, suggesting that the SPLET pathway became thermodynamically accessible, while in pentylethanoate, O17 remained the most favourable site with a PA of 68.43 kcal/mol.

The Gibbs free energy change (ΔG) provides a comprehensive measure of the spontaneity of antioxidant reactions. As shown in Figure 2, ΔG values varied markedly across the gas phase, water, and pentylethanoate environments. In the gas phase, positive ΔG values (6.46 kcal/mol at O16, 2.23 kcal/mol at O17, and 5.43 kcal/mol at O21) indicate that antioxidant reactions were energetically unfavourable under nonpolar conditions, though O17 again emerged as the most reactive site. In aqueous solution, ΔG values decreased substantially, with O16 at −2.07 kcal/mol, O17 at −4.41 kcal/mol, and O21 at 1.96 kcal/mol, confirming that the antioxidant process at O17 was highly favoured in polar environments. In pentylethanoate, ΔG values were 3.92 kcal/mol (O16), −0.68 kcal/mol (O17), and 2.64 kcal/mol (O21), with O17 once more exhibiting the only negative ΔG, highlighting its unique reactivity in lipid environments.

Overall, thermodynamic analysis underscored the environment-dependent antioxidant potential of AL. While gas-phase reactions were largely unfavourable, polar solvents significantly enhanced the thermodynamic profile, particularly at the O17 position. Collectively, the moderate BDE, markedly reduced IP in polar media, and favourable PA and ΔG values highlight AL's multifaceted antioxidant capacity, with fHAT and SET-PT emerging as the predominant mechanisms. Among the evaluated sites, O17 consistently stood out as the most reactive centre, owing to its advantageous energetic landscape across all mechanistic pathways.

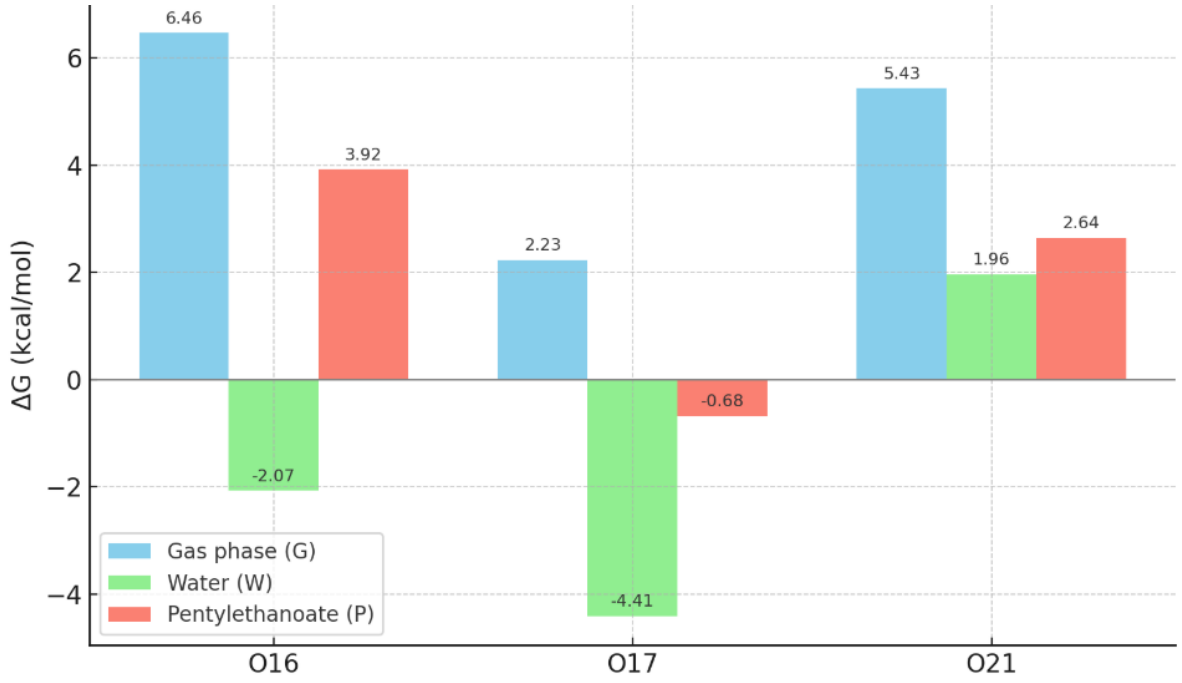

Figure 2. The free energies (kcal/mol) of AL calculated in gas, water, and pentyl ethanoate phases at the M05-2X/6–311++G(d,p) level of theory.

Table 1. BDE, IP, and PA values of the OH positions in the AL molecule in water and pentylethanoate.

Parameter	Site	Enthalpy (kcal/mol)		
		Gas phase	Water	Pentylethanoate
BDE	AL-O16	91.98	86.12	88.96
	AL-O17	86.75	83.21	83.75
	AL-O21	88.17	89.85	87.58
PA	AL-O16	234.41	13.91	20.51
	AL-O17	229.18	11.00	15.29
	AL-O21	230.60	17.64	19.13
IP	AL	171.63	115.30	127.42

Reaction Kinetics

In aqueous media, two main reaction mechanisms were investigated for compound AL: the hydrogen atom transfer (HAT) mechanism and the single electron transfer (SET) mechanism. AL possessed two active hydroxyl groups at positions 16 and 17; therefore, both sites were evaluated for their reactivity toward the $HOO^{\cdot}$ radical (Figure 3). For the SET mechanism, results showed that the OH group at position 17 reacted significantly more effectively than the OH at position 16. Specifically, the activation free energy ($\Delta G^{\neq}$) for the SET reaction at position 17 was only 4.5 kcal/mol, notably lower than the 7.6 kcal/mol observed at position 16. This led to a nearly two-order-of-magnitude higher apparent rate constant (k_{app}) at position 17. The reaction efficiency (Γ) at position 17 reached 93.6, compared to only 6.4 at position 16, indicating that position 17 played the dominant role in the SET-mediated radical scavenging activity of AL. This enhanced reactivity at O17 suggests that this hydroxyl site may act as the primary reactive centre in biological systems, contributing the most to the neutralization of reactive oxygen species and strengthening the overall antioxidant capacity of AL. In contrast, under the HAT mechanism, both hydroxyl sites exhibited relatively high activation free energies (21.7 kcal/mol at 16-OH and 16.3 kcal/mol at 17-OH) and low apparent rate constants (k_{app} of 2.1 and 5.1 $\times 10^2$ $M^{-1}.s^{-1}$, respectively). Notably, the reaction efficiency at both positions in aqueous media was 0, indicating that the HAT mechanism did not contribute significantly to the antioxidant activity of AL in water. It is worth noting that AL exhibited a total rate constant ($k_{overall}$) of 1.28×10^7 $M^{-1}\cdot s^{-1}$, indicating superior radical-scavenging performance in water compared to the known reference compound Trolox ($k = 8.96 \times 10^4$ $M^{-1}\cdot s^{-1}$) [27].

However, in an organic medium such as pentylethanoate, the HAT reaction at the 17-OH position of AL showed entirely different behaviour, as observed in Table 2. Although the activation energy remained moderate ($\Delta G^{\neq}$ = 17.2 kcal/mol), the reaction efficiency reached its maximum (Γ = 100), demonstrating that a non-polar environment made the HAT mechanism more effective at position 17. On the other hand, the SET mechanism was not observed in the pentylethanoate solvent, primarily due to its low dielectric constant and weak polarity. The SET process requires a highly polar environment to stabilize the charged intermediates formed during electron transfer, such as ions or charged radicals. In a non-polar organic solvent like pentylethanoate, these charged states are poorly stabilized, resulting in high energy barriers that render the SET reaction both kinetically and thermodynamically unfavourable. Therefore, in such an environment, the HAT mechanism becomes the dominant reaction pathway for compound AL.

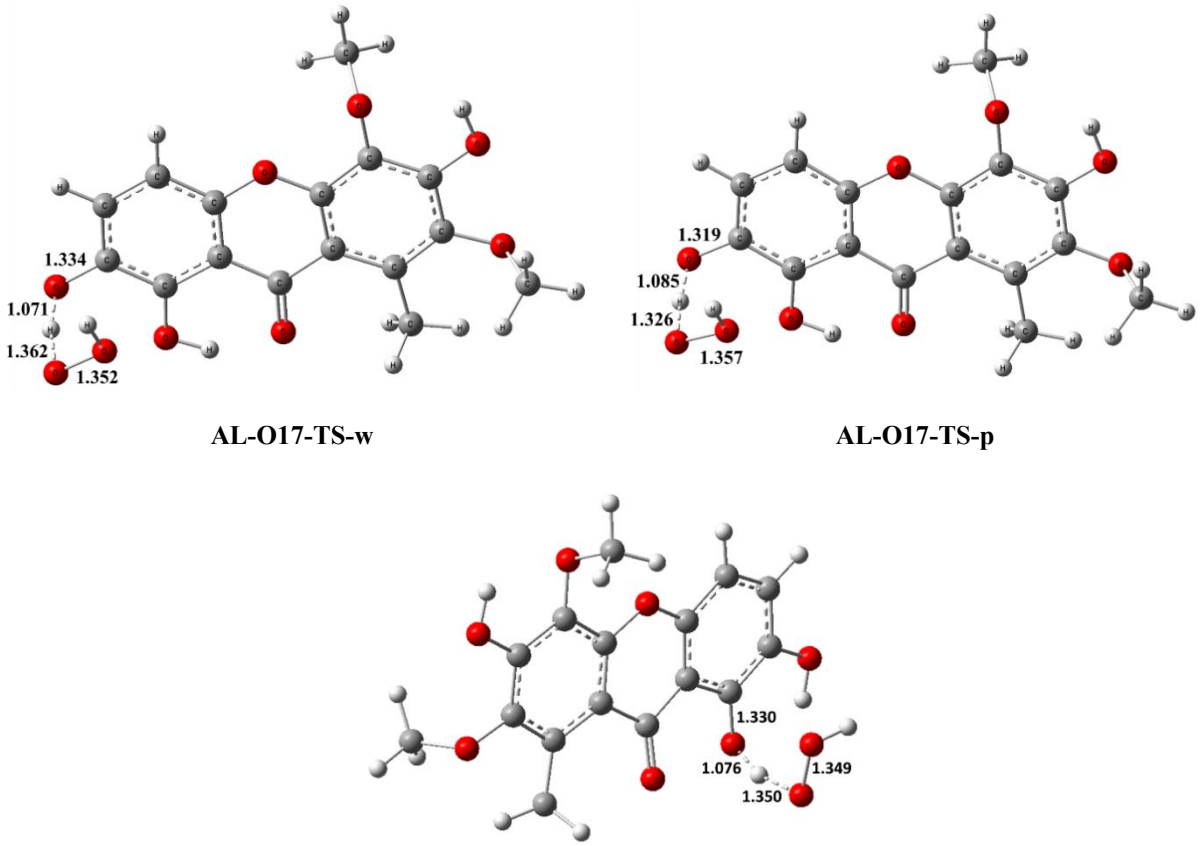

AL-O17-TS-w **AL-O17-TS-p**

AL-O16-TS-p

Figure 3. Transition state of the fHAT reaction between the 16- and 17- hydroxyl groups of AL and the HOO˙ radical in water (w) and pentylethanoate (p) media.

Table 2. Kinetic results of fHAT and SET reactions at selected hydroxyl groups of AL with the HOO˙ radical in water and pentylethanoate phases.

Mechanisms		**ΔG≠**	**κ/λ**	**k_{app}**	**k_f**	**Γ**	**$k_{overall}$**
Water							
16-O	SET	7.6	17.1	1.7×10^{7}	8.2×10^{5}	6.4	1.28×10^{7}
17-O	SET	4.5	16.2	1.3×10^{9}	1.2×10^{7}	93.6	
16-OH	fHAT	21.7	2874.5	2.1×10^{0}	4.76×10^{-2}	0.0	
17-OH	fHAT	16.3	70.0	5.1×10^{2}	4.5×10^{0}	0.0	
Pentylethanoate							
17-OH	fHAT	17.2	23.8	3.4×10^{1}		100	3.4×10^{1}

Molecular Docking and Dynamics

Keap1 (Kelch-like ECH-associated protein 1) is a crucial protein involved in regulating the body's antioxidant response through the Nrf2-Keap1 signaling pathway. Inhibiting Keap1 promotes the activation of Nrf2, a transcription factor that controls the expression of antioxidant and detoxification genes, thereby protecting cells from oxidative stress and damage caused by free radicals [6, 9]. This mechanism plays a vital role in preventing oxidative stress-related chronic diseases, including cancer, cardiovascular diseases,

and neurological disorders. Additionally, Nrf2 enhances the body's detoxification capacity, highlighting the therapeutic potential of Keap1 inhibition in developing new treatment strategies. In this study, molecular docking simulations were performed to explore the antioxidant mechanisms of compound AL in inhibiting the Keap1 protein (PDB ID: 4L7B). To validate the docking protocol, the co-crystal ligand 1VV was re-docked into the Keap1 binding site, yielding an RMSD value of 0.215 Å, thus confirming the reliability of the docking procedure [28]. The docking results showed that AL exhibited a binding affinity of –9.108 kcal/mol and formed several key stabilizing interactions within the Keap1 binding pocket, including hydrogen bonds with Tyr334, Ser363, and Ser602, π-π stacked and π-π T-shaped interactions with Tyr572 and Tyr334, and π-alkyl interactions with Tyr334 (Figure 4). Compared to 1VV, which also interacted with key residues such as Arg415, Ser363, and Tyr334, AL exhibited a similar interaction profile, particularly through its engagement with Tyr334 and Ser363. These residues are known to participate in the anchoring of Nrf2's ETGE motif to the Keap1 Kelch domain; thus, AL's interaction with Tyr334 and Ser363 may competitively disrupt this interface, facilitating the release and nuclear translocation of Nrf2. These overlapping interactions suggest that AL may effectively occupy the Keap1 binding pocket and disrupt the Keap1-Nrf2 interaction, thereby contributing to Nrf2 activation. Furthermore, when benchmarked against natural compounds previously reported as Keap1 inhibitors, AL displayed a higher binding affinity than those of several xanthones and related molecules, such as sterigmatocystin (–8.991 kcal/mol), 2,3,4,6,8-pentahydroxy-1-methylxanthone (–8.956 kcal/mol), 1,4,5-trihydroxy-2-methylxanthone (–8.917 kcal/mol), and 1,4,7-trihydroxy-6-methylxanthone (–8.848 kcal/mol) [6]. AL also outperformed other known antioxidants including gallic acid (–6.2 kcal/mol), coumaric acid (–5.8 kcal/mol), catechin (–8.4 kcal/mol), and epicatechin (–8.5 kcal/mol) [29].

While molecular docking provides valuable static insights into binding affinity and interaction networks, it does not capture the dynamic behaviour of the protein-ligand complex under physiological conditions [30, 31]. Therefore, the molecular docking simulation results were further analyzed through molecular dynamics (MD) simulations to assess the stability and durability of the Keap1-AL complex in a defined environment. RMSD values were calculated to evaluate the overall stability of the protein and ligand during the simulation, as shown in Figure 5. The RMSD analysis of the protein backbone indicated that the Keap1-AL complex maintained notable stability throughout the MD simulation period, with an average RMSD value of 0.3356 nm, comparable to the reference system Keap1-1VV and the unbound Keap1 protein. In terms of ligand stability, the RMSD analysis of AL in the Keap1-AL complex revealed an average value of 0.0595 nm. These minimal RMSD fluctuations reflect the ligand's stable conformation within the binding pocket, similar to the reference system. Overall, the Keap1-AL complex exhibited high structural stability, reinforcing its potential as a promising Keap1 inhibitor candidate capable of mediating Nrf2 activation and enhancing antioxidant defense mechanisms.

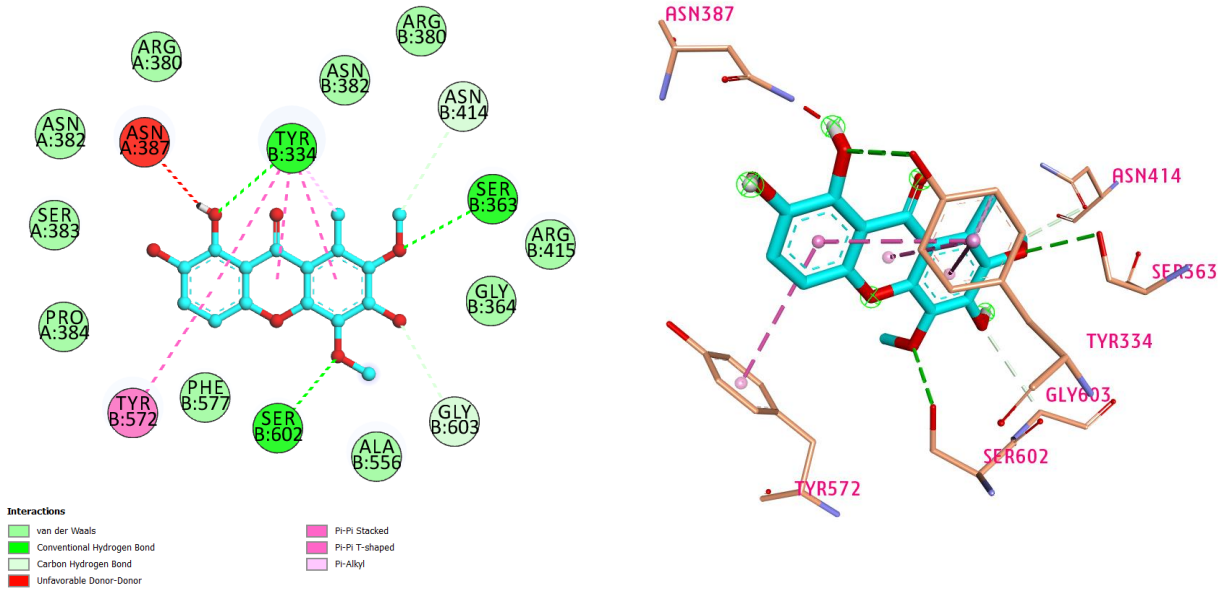

AL-4L7B

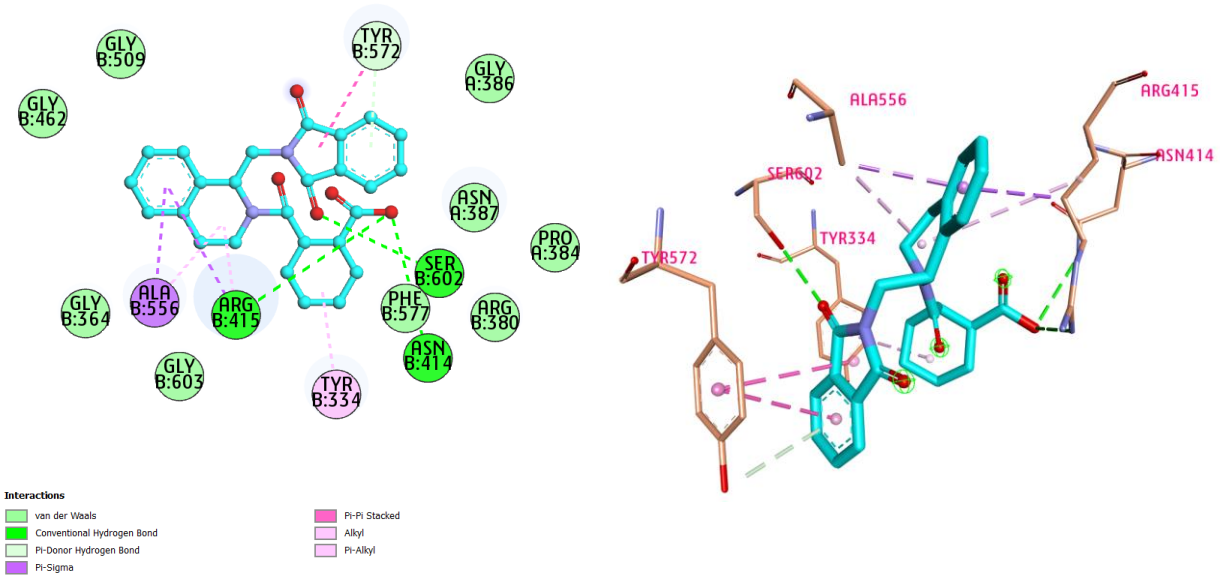

1VV-4L7B

Figure 4. Two-dimensional and three-dimensional interaction profiles of compound AL within the active site of the Keap1 protein (PDB ID: 4L7B).

ADMET Profile

To evaluate the pharmacokinetic and toxicity properties (ADMET) of compound AL, we utilized pkCSM, a predictive computational platform based on graph-based signatures and machine learning [22]. pkCSM enables accurate *in silico* prediction of a wide range of ADMET parameters solely from the chemical structure of a compound, making it an invaluable tool in early-stage drug discovery and candidate optimization. From Table 3, compound AL was predicted to demonstrate excellent oral absorption, with a human intestinal absorption rate of 91.8%. However, its poor water solubility (log S = -3.387) may limit its bioavailability. The compound exhibited moderate permeability across Caco-2 cells (log Papp = 0.441), and low skin permeability (log Kp = -2.744), indicating that transdermal delivery would be inefficient. Being a P-glycoprotein (P-gp) substrate, AL may be subject to efflux from intestinal epithelial cells, potentially reducing its intracellular concentration. However,

it did not inhibit either P-gp I or II, minimizing the risk of transporter-related drug interactions. In terms of distribution, AL showed a moderate volume of distribution (VDss = 0.167 log L/kg) and a low fraction unbound in plasma (Fu = 0.1), suggesting strong plasma protein binding and limited free drug availability. Its ability to cross the blood–brain barrier was poor (log BB = -1.247), and it showed minimal CNS penetration (log PS = -3.232), indicating limited central nervous system activity. During metabolism, AL was not a substrate for key cytochrome P450 enzymes CYP3A4 and CYP2D6, which could reduce the risk of rapid hepatic metabolism. However, it was predicted to inhibit CYP1A2, raising the potential for drug–drug interactions if co-administered with compounds metabolized by this enzyme. AL did not inhibit CYP2C19, CYP2C9, or CYP2D6. In terms of excretion, AL exhibited a moderate total clearance rate (log CL = 0.533 log ml/min/kg) and was not a substrate of the renal transporter OCT2, suggesting that renal elimination may not be a major pathway. The toxicity profile revealed a few concerns. AL tested positive in the Ames test, indicating potential mutagenicity. However, it did not inhibit hERG I or II channels, suggesting a low risk of cardiotoxicity. The compound had moderate acute toxicity in rats (LD_{50} = 1,802 mol/kg) and chronic toxicity (LOAEL = 2.174 log mg/kg_bw/day). It was not predicted to be hepatotoxic or a skin sensitizer, indicating good systemic and dermal safety. Its environmental toxicity level was moderate, with measurable effects on *Tetrahymena pyriformis* and minnow species. Importantly, the drug-likeness evaluation supported the ADMET profile of AL. It satisfied all major drug-like rules, including Lipinski's rule of five (0 violations), as well as the Ghose, Veber, Egan, and Muegge criteria, suggesting that its physicochemical properties were within the acceptable range for oral drugs (Table 4).

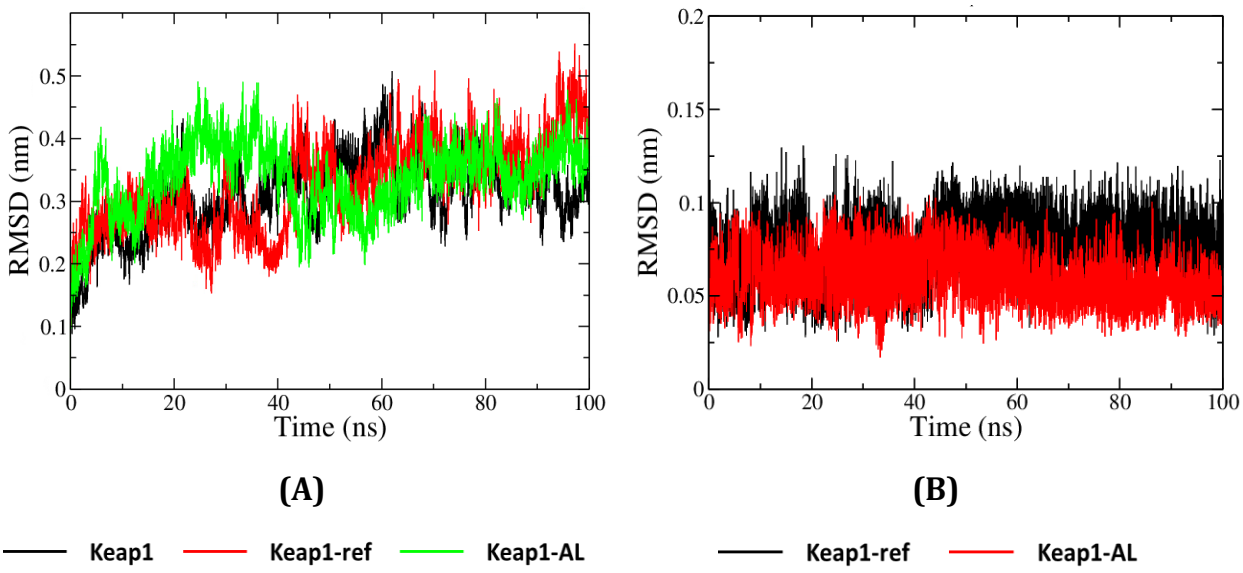

Figure 5. RMSD plots of (A) the protein backbone and (B) the ligand over 100 ns of molecular dynamics (MD) simulation.

Table 3. ADMET profiles of AL.

Property	**Model Name**	**Predicted Value**	**Unit**
Absorption	Water solubility	-3,387	Numeric (log mol/L)
	Caco2 permeability	0.441	Numeric (log Papp in 10^{-6} cm/s)
	Intestinal absorption (human)	91,804	Numeric (% Absorbed)
	Skin Permeability	-2,744	Numeric (log Kp)
	P-glycoprotein substrate	Yes	Categorical (Yes/No)
	P-glycoprotein I inhibitor	No	Categorical (Yes/No)
	P-glycoprotein II inhibitor	No	Categorical (Yes/No)
Distribution	VDss (human)	0.167	Numeric (log L/kg)
	Fraction unbound (human)	0.1	Numeric (Fu)
	BBB permeability	-1,247	Numeric (log BB)
	CNS permeability	-3,232	Numeric (log PS)
Metabolism	CYP2D6 substrate	No	Categorical (Yes/No)
	CYP3A4 substrate	No	Categorical (Yes/No)
	CYP1A2 inhibitior	Yes	Categorical (Yes/No)
	CYP2C19 inhibitior	No	Categorical (Yes/No)
	CYP2C9 inhibitior	No	Categorical (Yes/No)
	CYP2D6 inhibitior	No	Categorical (Yes/No)
	CYP3A4 inhibitior	No	Categorical (Yes/No)
Excretion	Total Clearance	0.533	Numeric (log ml/min/kg)
	Renal OCT2 substrate	No	Categorical (Yes/No)
Toxicity	AMES toxicity	Yes	Categorical (Yes/No)
	Max. tolerated dose (human)	0.514	Numeric (log mg/kg/day)
	hERG I inhibitor	No	Categorical (Yes/No)
	hERG II inhibitor	No	Categorical (Yes/No)
	Oral Rat Acute Toxicity (LD_{50})	1,802	Numeric (mol/kg)
	Oral Rat Chronic Toxicity (LOAEL)	2,174	Numeric (log mg/kg_bw/day)
	Hepatotoxicity	No	Categorical (Yes/No)
	Skin Sensitisation	No	Categorical (Yes/No)
	T.Pyriformis toxicity	0.386	Numeric (log µg/L)
	Minnow toxicity	1,414	Numeric (log mM)

Table 4. Physicochemical Properties, Lipophilicity, and Drug-likeness of AL.

No.	Parameters	Predicted Value
1	Formula	$C_{15}H_{12}O_7$
2	Molecular weight	304.25 g/mol
3	Number of heavy atoms	22
4	Number of aromatic heavy atoms	14
5	Fraction Csp3	0.13
6	Number of rotatable bonds	2
7	Number of hydrogen bond acceptors	7
8	Number of hydrogen bond donors	3
9	Molar refractivity	79.04
10	TPSA	109.36 $Å^2$
11	Consensus Log $P_{o/w}$	1.76
12	Lipinski	Yes; 0 violation
13	Ghose	Yes
14	Veber	Yes
15	Egan	Yes
16	Muegge	Yes

CONCLUSION

In this study, we carried out a comprehensive computational analysis to clarify the antioxidant potential of aspidxanthone A (AL), a newly isolated xanthone derivative from *Aspidistra letreae*. Thermodynamic and kinetic analyses showed that AL engaged in different antioxidant mechanisms depending on the surrounding environment, with the SET pathway being dominant in aqueous conditions while the HAT mechanism prevailed in lipid-like environments. Among the hydroxyl groups, the O17 position consistently emerged as the most reactive site across all mechanisms. Molecular docking and molecular dynamics simulations further supported AL's strong affinity for the Keap1 protein and the stability of the Keap1–AL complex. These findings indicate that AL may interfere with the Keap1–Nrf2 interaction and help enhance endogenous antioxidant defences. ADMET predictions indicated that AL possessed favourable pharmacokinetic properties and an overall acceptable safety profile, although some limitations such as potential mutagenicity warrant further investigation. Collectively, these findings highlight AL as a promising antioxidant candidate whose mechanisms were medium-dependent,

exhibiting direct radical-scavenging activity and indirect antioxidant potential through Keap1 inhibition. Looking forward, experimental validation through both *in vitro* and *in vivo* assays is essential to confirm the predicted antioxidant mechanisms and Keap1 inhibitory activity. Additionally, structural modification of AL could be explored to minimize mutagenicity while maintaining its redox efficacy. Future studies may also employ QSAR-based optimization to design AL analogues with enhanced potency and improved safety profiles. This work provides a solid theoretical foundation for future *in vitro* and *in vivo* studies, advancing the development of AL-based therapeutics for oxidative stress-related diseases.

ACKNOWLEDGEMENTS

Author Contributions

Hoang Thi Tue Trang, Ngu Thi Tra Giang – methodology, data curation, formal analysis, writing-editing, visualization, Nguyen Ngoc Anh Thu – investigations, data curation, formal analysis, visualization, writing-original draft, conceptualization, resources, supervision, writing- editing.

Conflicts of Interest

There are no conflicts of interest to declare.

Funding

No funding was received for conducting this study.

REFERENCES

1. Leonid, V., Tillich, H. J. and Tuan, A. (2017) Aspidistra letreae (Asparagaceae), a new species from central Vietnam. *Phytotaxa*, **308(1)**, 137–140.

2. Ho, D. V., Hoang, H. N. T., Vo, H. Q., Nguyen, K. V., Pham, T. V., Le, A. T. and Nguyen, H. T. (2020) Three new steroidal saponins from Aspidistra letreae plants and their cytotoxic activities. *Journal of Natural Medicines*, **74(3)**, 591–598.

3. Ho, D. V., Hoang, H. N. T., Vo, K. M., Le, A. T. and Nguyen, H. T. (2020) Chemical constituents and cytotoxicity of Aspidistra letreae. *Hue University Journal of Science: Natural Science*, **129(1B)**, 31–39.

4. Ho, D. V., Nguyen, H. T., Vu, T. Y., Pham, T. V. and Nguyen, H. M. (2021) Antioxidant activity of a new xanthone derivative from Aspidistra letreae: in vitro and in silico studies. *Chemistry & Biodiversity*, **18(4)**, e2001008.

5. Nguyen, H. M., Nguyen, H. T., Seephan, S., Do, H. B., Nguyen, H. T., Ho, D. V., and Pongrakhananon, V. (2021) Antitumor activities of Aspiletrein A, a steroidal saponin from Aspidistra letreae, on non-small cell lung cancer cells. *BMC Complementary Medicine and Therapies*, **21(1)**, 87.

6. Thuy, P. T. and Ha, N. X. (2024) Theoretical studies on the antioxidant activity of potential marine xanthones. *Free Radical Research*, **58(12)**, 826–840.

7. Martínez, A., Hernández-Marin, E. and Galano, A. (2012) Xanthones as antioxidants: A theoretical study on the thermodynamics and kinetics of the single electron transfer mechanism. *Food & Function*, **3(4)**, 442–450.

8. Male, Y. T., Sutapa, I. W., Maahury, M. F. and Kailola, F. (2023) Computational study anti-oxidant properties of xanthone-derivatives from mangosteen (Garcinia mangostana L.) pericarp using density functional theory (DFT). *AIP Conference Proceedings*, **2588(1)**, 020018.

9. Kaspar, J. W., Niture, S. K. and Jaiswal, A. K. (2009) Nrf2: INrf2 (Keap1) signaling in oxidative stress. *Free Radical Biology and Medicine*, **47(9)**, 1304–1309.

10. Marenich, A. V., Cramer, C. J. and Truhlar, D. G. (2009) Universal solvation model based on solute electron density and on a continuum model of the solvent defined by the bulk dielectric constant and atomic surface tensions. *The Journal of Physical Chemistry B*, **113(18)**, 6378–6396.

11. Marković, Z., Tošović, J., Milenković, D. and Marković, S. (2016) Revisiting the solvation enthalpies and free energies of the proton and electron in various solvents. *Computational and Theoretical Chemistry*, **1077**, 11–17.

12. Frisch, M. J., Trucks, G. W., Schlegel, H. B., Scuseria, G. E., Robb, M. A., Cheeseman, J. R., Scalmani, G., Barone, V., Petersson, G. A., Nakatsuji, H., Li, X., Caricato, M., Marenich, A. V., Bloino, J., Janesko, B. G., Gomperts, R., Mennucci, B., Hratchian, H. P., Ortiz, J. V., Izmaylov, A. F., Sonnenberg, J. L., Williams-Young, D., Ding, F., Lipparini, F., Egidi, F., Goings, J., Peng, B., Petrone, A., Henderson, T., Ranasinghe, D., Zakrzewski, V. G., Gao, J., Rega, N., Zheng, G., Liang, W., Hada, M., Ehara, M., Toyota, K., Fukuda, R., Hasegawa, J., Ishida, M., Nakajima, T., Honda, Y., Kitao, O., Nakai, H., Vreven, T., Throssell, K., Montgomery, J. A., Peralta, J. E., Ogliaro, F., Bearpark, M. J., Heyd, J. J., Brothers, E. N., Kudin, K. N., Staroverov, V. N., Keith, T. A., Kobayashi, R., Normand, J., Raghavachari, K., Rendell, A. P., Burant, J. C., Iyengar, S. S., Tomasi, J., Cossi, M., Millam, J. M., Klene, M., Adamo, C., Cammi, R., Ochterski, J.

W., Martin, R. L., Morokuma, K., Farkas, O., Foresman, J. B. and Fox, D. J. (2016) Gaussian 16 Rev. B.01, Wallingford CT: Gaussian Inc.

13. Jnoff, E., Albrecht, C., Barker, J. J., Barker, O., Beaumont, E., Bromidge, S. and Courade, J. P. (2014) Binding mode and structure–activity relationships around direct inhibitors of the Nrf2–Keap1 complex. *ChemMedChem*, **9(4)**, 699–705.

14. Eberhardt, J., Santos-Martins, D., Tillack, A. F. and Forli, S. (2021) AutoDock Vina 1.2. 0: new docking methods, expanded force field, and python bindings. *Journal of Chemical Information and Modeling*, **61(8)**, 3891–3898.

15. Ha, N. X. and Le, C. H. (2024) In silico molecular docking and ADMET study of Isodon coetsa phytochemicals targeting TNF-α in inflammation-mediated diseases. *Vietnam Journal of Chemistry*, **62(3)**, 387–393.

16. Hoang Minh Chau, C., Thi Tra Giang, N., Thi Thuy Tram, N., Thi My Chau, L., Xuan Ha, N. and Thi Thuy, P. (2024) In silico molecular docking and molecular dynamics of Prinsepia utilis phytochemicals as potential inhibitors of phosphodiesterase 4B. *Journal of Chemical Research*, **48(6)**, 17475198241305879.

17. Van Der Spoel, D., Lindahl, E., Hess, B., Groenhof, G., Mark, A. E. and Berendsen, H. J. (2005) GROMACS: fast, flexible, and free. *Journal of computational chemistry*, **26(16)**, 1701–1718.

18. Lindorff-Larsen, K., Piana, S., Palmo, K., Maragakis, P., Klepeis, J. L., Dror, R. O. and Shaw, D. E. (2010) Improved side-chain torsion potentials for the Amber ff99SB protein force field. *Proteins: Structure, Function, and Bioinformatics*, **78(8)**, 1950–1958.

19. Wang, J., Wolf, R. M., Caldwell, J. W., Kollman, P. A. and Case, D. A. (2004) Development and testing of a general amber force field. *Journal of Computational Chemistry*, **25(9)**, 1157–1174.

20. Case, D. A., Aktulga, H. M., Belfon, K., Cerutti, D. S., Cisneros, G. A., Cruzeiro, V. W. D., et al. (2023) AmberTools. *Journal of Chemical Information and Modelling*, **63(20)**, 6183–6191.

21. Hess, B., Bekker, H., Berendsen, H. J. and Fraaije, J. G. (1997) LINCS: A linear constraint solver for molecular simulations. *Journal of Computational Chemistry*, **18(12)**, 1463–1472.

22. Pires, D. E., Blundell, T. L. and Ascher, D. B. (2015) pkCSM: predicting small-molecule pharmacokinetic and toxicity properties using graph-based signatures. *Journal of Medicinal Chemistry*, **58(9)**, 4066–4072.

23. Duque, L., Guerrero, G., Colorado, J. H., Restrepo, J. A. and Velez, E. (2022) Theoretical Insight into mechanism of antioxidant capacity of atorvastatin and its o-hydroxy and p-hydroxy metabolites, using DFT methods. *Computational and Theoretical Chemistry*, **1214**, 113758.

24. Thuy, P. T., Ha, N. X. and Hue, N. T. M. (2025) Theoretical studies on the radical scavenging activity of dioxinodehydroeckol. *Structural Chemistry*, 1–7.

25. Vargas-Sánchez, R. D., Mendoza-Wilson, A. M., Torrescano-Urrutia, G. R. and Sánchez-Escalante, A. (2015) Antiradical potential of phenolic compounds fingerprints of propolis extracts: DFT approach. *Computational and Theoretical Chemistry*, **1066**, 7–13.

26. Hossen, J., Ali, M. A. and Reza, S. (2021) Theoretical investigations on the antioxidant potential of a non-phenolic compound thymoquinone: a DFT approach. *Journal of Molecular Modelling*, **27(6)**, 173.

27. Alberto, M. E., Russo, N., Grand, A. and Galano, A. (2013) A physicochemical examination of the free radical scavenging activity of Trolox: mechanism, kinetics and influence of the environment. *Physical Chemistry Chemical Physics*, **15(13)**, 4642–4650.

28. Keomanykham, O., Van Nguyen, H., Phuong Hoa, L. T., Ha, N. X., Xangyaorn, B., Thi Nguyen, H. M. and Quang, D. N. (2025) Structures and Properties of Phenylethanoid Glycosides from Barleria prionitis Linn.: Insights from Theoretical and Experimental Investigations. *Acta Chimica Slovenica*, **72(1)**.

29. Diniyah, N., Alam, M. B., Javed, A., Alshammari, F. H., Choi, H. J. and Lee, S. H. (2023) In silico and docking studies on the binding activities of Keap1 of antioxidant compounds in non-oilseed legumes. *Arabian Journal of Chemistry*, **16(1)**, 104414.

30. Singh, S., Baker, Q. B. and Singh, D. B. (2022) Molecular docking and molecular dynamics simulation. In *Bioinformatics*, 291–304.

31. Morris, C. J. and Corte, D. D. (2021) Using molecular docking and molecular dynamics to investigate protein-ligand interactions. *Modern Physics Letters B*, **35(08)**, 2130002.